IOPscience iopscience.iop.org

Home Search Collections Journals About Contact us My IOPscience

Origin of tunneling lineshape trends for Kondo states of Co adatoms on coinage metal surfaces

This article has been downloaded from IOPscience. Please scroll down to see the full text article.

2009 J. Phys.: Condens. Matter 21 355501

(http://iopscience.iop.org/0953-8984/21/35/355501)

View the table of contents for this issue, or go to the journal homepage for more

Download details:
IP Address: 129.252.86.83
The article was downloaded on 29/05/2010 at 20:49

Please note that terms and conditions apply.

IOP PUBLISHING JOURNAL OF PHYSICS: CONDENSED MATTER

J. Phys.: Condens. Matter **21** (2009) 355501 (8pp) doi:10.1088/0953-8984/21/35/355501

Origin of tunneling lineshape trends for Kondo states of Co adatoms on coinage metal surfaces

Sahar Sharifzadeh[1], **Patrick Huang**[2] **and Emily A Carter**[3]

[1] Department of Electrical Engineering, Princeton University, Princeton, NJ 08544-5263, USA
[2] Physics and Life Sciences Directorate, Lawrence Livermore National Laboratory, Livermore, CA 94551, USA
[3] Department of Mechanical and Aerospace Engineering and Program in Applied and Computational Mathematics, Princeton University, Princeton, NJ 08544-5263, USA

E-mail: eac@princeton.edu

Received 22 April 2009, in final form 25 June 2009
Published 7 August 2009
Online at stacks.iop.org/JPhysCM/21/355501

Abstract

Embedded correlated wavefunction (ECW) theory is used to characterize the Kondo states formed by Co atoms adsorbed on Ag(111) and Ag(100). Clusters containing the adatom are described with CW theory, while effects of the extended crystal are included via an embedding potential. The predicted Co d-electronic structure, combined with earlier predictions for Co on Cu surfaces, explains the different tunneling behavior observed with the scanning tunneling microscope (STM) for Co adsorbed on different coinage metal surfaces.

1. Introduction

The Kondo effect refers to a set of a low-temperature, strongly correlated electron phenomena involving magnetic impurities in non-magnetic metal host crystals [1]. Early observations of the effect came from measurements of the low-temperature resistivity in such samples; as the temperature T decreases, their resistivity approaches a minimum followed by an increase with a $-\ln T$ dependence, in contrast to the typical behavior for metals (monotonically decreasing resistivity). Kondo was able to explain this anomalous behavior by assuming that the impurity spin(s) anti-ferromagnetically couple(s) with the conduction electrons, forming a many-body resonance state at the Fermi level responsible for altering the resistivity of the material [2]. Subsequent experiments confirmed that magnetic quenching occurs below a characteristic temperature T_K (the Kondo temperature), as evidenced by a constant magnetic susceptibility as $T \rightarrow 0$ [3]. Decades after this suggestion, direct evidence for the Kondo resonance was provided by scanning tunneling spectroscopy (STS) studies of magnetic adatoms on metal surfaces [4, 5], generating renewed interest in understanding the electronic structure of the surface Kondo effect.

The Kondo state on surfaces manifests as a resonance near the Fermi energy in the STS [6, 7], whose lineshape can be modeled as arising from Fano-type tunneling to a discrete impurity state embedded in a continuum [8]. The asymmetry in the lineshape is attributed to the interference between the two tunneling pathways available: tunneling to the adsorbate and tunneling to the continuum of conduction electron states. Within this model, the lineshape takes the form [6]

$$\frac{\mathrm{d}I}{\mathrm{d}V} \propto \frac{(\varepsilon' + q)^2}{1 + \varepsilon'^2}, \qquad \varepsilon' = \frac{eV + \Delta\varepsilon}{k_B T_K} \tag{1}$$

where V is the applied bias, $\Delta\varepsilon$ is a small shift in the Kondo resonance from the Fermi level and $k_B T_K$ is related to the width of the resonance. The asymmetry parameter q can be interpreted as the ratio of the probability of tunneling to the adsorbate to the probability of tunneling to the continuum. If tunneling to the continuum dominates the tunneling pathway ($q \sim 0$), the lineshape will be symmetric around the minimum. If tunneling occurs to the adsorbate and the continuum ($q \sim 1$), the lineshape is asymmetric.

The parameters q and T_K are found by fitting to the STS data, and systematic variations of the substrate yield different parameter values with no obvious trend with surface element or orientation. This is illustrated in table 1 for cobalt (Co) adatoms on coinage metal surfaces. We are particularly interested in understanding the large variation of the asymmetry parameter q, which directly signals tunneling mechanism changes. The STS lineshape is asymmetric for

© 2009 IOP Publishing Ltd Printed in the UK

Table 1. The Kondo temperature T_K and q parameter for Co atoms adsorbed on non-magnetic transition metal surfaces, as determined by fitting equation (1) to the STS lineshape.

	T_K	Type of lineshape	q
Co/Cu(111)[a]	54 ± 2	Nearly symmetric dip	0.2
Co/Cu(100)[a]	88 ± 4	Asymmetric dip	1.1
Co/Ag(111)[b]	92 ± 6	Symmetric dip	0
Co/Ag(100)[c]	41 ± 5	Symmetric dip	0
Co/Au(111)[d]	75 ± 6	Asymmetric dip	0.6

[a] Reference [9]. [b] Reference [10]. [c] Reference [11].
[d] Reference [6].

Co on Cu(100) and Au(111) but is symmetric for Co on Cu(111), Ag(111) and Ag(100) [6, 9–11]. The fact that the asymmetry parameter and therefore the tunneling mechanism is different for Co on these different surfaces suggests that the host metal strongly influences the local electronic structure near the impurity atom. Neither coordination number around Co (three or four) nor host metal identity (Cu, Ag or Au) reveals a trend. For example, why does Co/Cu(100) not have a similar lineshape to Co/Cu(111)—same host element—or Co/Ag(100)—same coordination number? These seemingly contradictory and rather mysterious observations motivate the present work, which aims to provide insight into the origin of these observations from an *ab initio* theory.

Theoretical work on the Kondo effect has been based largely on the Anderson impurity model [12], with the use of empirical and/or density functional theory (DFT)-based input parameters [13–19]. Here the impurity is typically treated as a single discrete state in a model band structure representing the surface. Important impurity parameters that need to be chosen include the d-orbital occupation n_d, on-site Coulomb repulsion U and impurity-conduction hybridization; ambiguities in the determination of these quantities for realistic impurities and surfaces have led to conflicting conclusions. Ideally, one would like a parameter-free description for the full electronic structure of the impurity and substrate that includes the many-body effects leading to formation of the Kondo state. This is a difficult task, as the usual DFT within the local density or gradient approximations have well-known problems when strong correlation effects are present.

Recently, Huang and Carter (HC) studied Co on Cu (111) and Cu(100) surfaces [20–22] with an embedded correlated wavefunction (ECW) method [20, 23–29]. Here the Co and nearby metal atoms are studied with highly accurate complete active space self-consistent field (CASSCF) and/or configuration interaction (CI) theory, allowing for explicit *ab initio* treatment of the impurity electronic structure and the local many-body effects that lead to formation of the Kondo resonance. The effects of the extended crystal on the Co/metal atom cluster are accounted for through a periodic DFT-based embedding potential, which approximates correlation effects from metallic electrons beyond the range of the cluster. Here no empirical model is used for the interactions; the only physical assumption made (other than that DFT describes metallic interactions well, which it does) is that the essential correlation effects are local. This is a fair assumption since the Kondo temperature has been shown to depend strongly on the local environment around the impurity [30, 31]. The work of HC was the first to predict *ab initio* the emergence of a many-body open-shell singlet ground state for the Kondo resonance, as was assumed by Kondo long ago in order to explain the resistivity minimum. Moreover, HC's comparison of the Kondo state wavefunctions formed by Co adsorbed on Cu(111) and Cu(100) strongly suggested that the internal d-structure on Co likely determines which tunneling mechanism is observed.

In this paper, we use the ECW method to investigate other surface Kondo states, with the goal of providing a more comprehensive understanding of the observed tunneling lineshapes. In particular, we compare Co adsorbed on Ag(111) and Ag(100) to the earlier ECW studies of Co/Cu(111) and Cu(100). We employ the new all-electron ECW method, which has been shown to reproduce the results of HC [29]. Our results for Co on Ag surfaces verify that the tunneling behavior of Co on Cu and Ag surfaces can be explained on the basis of the effective Co d-orbital occupations derived from the many-body wavefunction. We shall also see that wavefunction analyses allow us to understand why Cu and Ag surfaces affect the Kondo resonance differently, i.e. why the resonance and corresponding tunneling lineshape is structure-sensitive on Cu but not on Ag surfaces.

2. Embedded correlated wavefunction (ECW) theory

The ECW theory transforms the general problem of treating a local feature in condensed matter into a correlated wavefunction problem for a cluster of atoms containing the feature, subject to an external embedding potential that accounts for the interactions with the surroundings. To this end, we partition the total system into region I, a region of interest consisting of a cluster of atoms containing the adsorbate and nearby metal atoms that are treated with CW theory, and region II, a background region whose nuclei and electron density are derived from projector augmented wave (PAW) [32] DFT calculations.

Formally, the total system's energy is written as $E_{\mathrm{tot}}[\rho_{\mathrm{tot}}] = E_{\mathrm{I}}[\rho_{\mathrm{I}}] + E_{\mathrm{II}}[\rho_{\mathrm{II}}] + E_{\mathrm{int}}$, where ρ_{I} and ρ_{II} are densities associated with regions I and II, respectively. E_{I} and E_{II} denote the exact, unknown energy density functionals associated with regions I and II and E_{int} is the exact, unknown interaction energy between the two regions. We employ an orbital-free DFT-based model for E_{int}:

$$E_{\mathrm{int}} = E_{\mathrm{tot}}^{\mathrm{DFT}}[\rho_{\mathrm{tot}}] - E_{\mathrm{I}}^{\mathrm{DFT}}[\rho_{\mathrm{I}}] - E_{\mathrm{II}}^{\mathrm{DFT}}[\rho_{\mathrm{II}}],$$

where the individual energy density functionals are decomposed in the usual DFT manner:

$$E_i^{\mathrm{DFT}} = T_s[\rho_i] + J[\rho_i] + E_{\mathrm{xc}}[\rho_i] + \int \mathrm{d}\mathbf{r}\, \rho_i(\mathbf{r}) \upsilon_{\mathrm{ion}}^i(\mathbf{r})$$

for $i = \mathrm{I}, \mathrm{II}, \mathrm{tot}$. Here, T_s, J and E_{xc} are the kinetic, Hartree and exchange–correlation energy density functionals, respectively, and $\upsilon_{\mathrm{ion}}^i$ is the external potential due to the nuclei in region i. Under the assumption that the background region is essentially unaffected by the adsorbate (i.e. $\delta E_{\mathrm{II}}/\delta\rho_{\mathrm{I}} = 0$, which will be true provided the cluster of region I is large enough), the embedding potential is constructed as [20, 29]

$$\begin{aligned}\upsilon_{\mathrm{emb}} &= \delta E_{\mathrm{int}}/\delta\rho_{\mathrm{I}}\\ &= \delta E_{\mathrm{tot}}/\delta\rho_{\mathrm{tot}} - \delta E_{\mathrm{I}}/\delta\rho_{\mathrm{I}}\\ &= \upsilon_{T_s}[\rho_{\mathrm{tot}},\rho_{\mathrm{I}}] + \upsilon_J[\rho_{\mathrm{tot}},\rho_{\mathrm{I}}] + \upsilon_{\mathrm{xc}}[\rho_{\mathrm{tot}},\rho_{\mathrm{I}}] + \upsilon_{\mathrm{ion}}^{\mathrm{II}}.\end{aligned}$$

We employ the Thomas–Fermi + 1/9 von Weizsäcker kinetic energy density functional and the local density approximation (LDA) [33] for exchange–correlation in υ_{emb}, both of which have been demonstrated to be accurate for metallic embedding [20, 27, 29]. In the latest version of the ECW theory [29], all-electron valence electron densities in region II are used in the construction of υ_{emb}. Then the electron–ion term in υ_{emb} associated with the background region, $\upsilon_{\mathrm{ion}}^{\mathrm{II}}$, is represented by a screened Coulomb potential in which the core electrons and nucleus of each atom are treated together as a point charge instead of by a pseudopotential, as had been used in earlier incarnations of the ECW theory [20, 24, 27]. As discussed elsewhere [29], the highly localized core electrons in region II do not contribute significantly to the embedding potential within region I; instead the core electrons are implicitly accounted for by the shape of the background valence density, which is optimized in the presence of frozen cores within the PAW–DFT method. The explicit inclusion of core electron densities in the embedding potential was shown to not significantly affect the resulting embedded density, wavefunction or energetics [29].

We begin the embedding procedure by constructing a background valence density $\rho_{\mathrm{II}}^{\mathrm{frozen}}$ from a Kohn–Sham PAW–DFT calculation on just the background region, which subsequently is kept fixed throughout the self-consistent embedding calculation. Alternatively, $\rho_{\mathrm{II}}^{\mathrm{frozen}}$ can be constructed as the difference between the densities of the total system and region I. The nature of the embedded wavefunction is insensitive to the method selected for background density construction [28]. An initial embedding potential is then formed from an initial region I density, ρ_{I}^{0}, and a total density $\rho_{\mathrm{tot}}^{0} = \rho_{\mathrm{I}}^{0} + \rho_{\mathrm{II}}^{\mathrm{frozen}}$, where ρ_{I}^{0} is constructed from a CW calculation on the 'bare' (non-embedded) cluster. Then the region I wavefunction is optimized in the presence of this initial embedding potential:

$$\left[H_{\mathrm{I}} + \sum_{j=1}^{N}\upsilon_{\mathrm{emb}}(\mathbf{r}_j)\right]\Psi_{\mathrm{I,emb}} = E\Psi_{\mathrm{I,emb}}.$$

H_{I} is the *ab initio* Hamiltonian describing the region I atoms and $\Psi_{\mathrm{I,emb}}$ is the many-electron wavefunction from which a new density ρ_{I}' can be derived from its natural orbitals. A new $\rho_{\mathrm{tot}} = \rho_{\mathrm{I}}' + \rho_{\mathrm{II}}^{\mathrm{frozen}}$ and a new $\upsilon_{\mathrm{emb}}(\rho_{\mathrm{I}}', \rho_{\mathrm{tot}})$ are then constructed and the cycle to obtain the embedded wavefunction $\Psi_{\mathrm{I,emb}}$ is repeated until self-consistency. The electronic structure of the converged embedded wavefunction is then analyzed.

The total energy of the embedded cluster and background can be defined as a correction to the total periodic DFT energy, $E_{\mathrm{tot}}^{\mathrm{DFT}}$, within region I as [24–28]

$$\begin{aligned}E_{\mathrm{tot}}^{\mathrm{emb}} &= E_{\mathrm{I}}^{\mathrm{CW}} + E_{\mathrm{II}}^{\mathrm{DFT}} + E_{\mathrm{int}}^{\mathrm{DFT}}\\ &= E_{\mathrm{I}}^{\mathrm{DFT}} + E_{\mathrm{II}}^{\mathrm{DFT}} + E_{\mathrm{int}}^{\mathrm{DFT}} + E_{\mathrm{I}}^{\mathrm{CW}} - E_{\mathrm{I}}^{\mathrm{DFT}}\\ &= E_{\mathrm{tot}}^{\mathrm{DFT}} + (E_{\mathrm{I}}^{\mathrm{CW}} - E_{\mathrm{I}}^{\mathrm{DFT}}).\end{aligned}$$

The region I CW ($E_{\mathrm{I}}^{\mathrm{CW}}$) and DFT ($E_{\mathrm{I}}^{\mathrm{DFT}}$) energies are evaluated without υ_{emb}, as described earlier, to avoid double counting of interactions already present in $E_{\mathrm{tot}}^{\mathrm{DFT}}$ [25–28]. $E_{\mathrm{I}}^{\mathrm{CW}}$ is evaluated from the embedded wavefunction as $\langle\Psi_{\mathrm{I,emb}}|H_{\mathrm{I}}|\Psi_{\mathrm{I,emb}}\rangle$. The DFT energies $E_{\mathrm{I}}^{\mathrm{DFT}}$ and $E_{\mathrm{tot}}^{\mathrm{DFT}}$ should always be evaluated from the ground state wavefunction, since the expression used in the above derivation:

$$E_{\mathrm{tot}}^{\mathrm{DFT}} = E_{\mathrm{I}}^{\mathrm{DFT}} + E_{\mathrm{II}}^{\mathrm{DFT}} + E_{\mathrm{int}}^{\mathrm{DFT}},$$

is only meaningful for the ground state DFT energy. Here, however, we are only interested in excited state energies relative to the ground state of a given cluster structure. Thus, these DFT terms cancel out in the calculation of excitation energies, and in practice for excitation energies we need only evaluate differences in $E_{\mathrm{I}}^{\mathrm{CW}}$.

3. Calculational details

3.1. Structural models

The geometries of Co adatoms on Ag surfaces were determined at the spin-polarized (SP) PAW–DFT–LDA level; these optimized geometries were used in the subsequent ECW calculations. All DFT calculations were performed with the Vienna *ab Initio* simulation package (VASP) [34], using the SP LDA exchange–correlation functional of Perdew and Zunger [33] and default PAW potentials for Co and Ag provided with the VASP code (9 valence electrons for Co and 11 valence electrons for Ag were treated self-consistently).

The slab models (figures 1(a) and (b)) used to determine the adsorbate–surface structures consisted of one Co atom adsorbed on one side of a four-layer, 3 × 3 Ag(111) periodic slab (9 atoms/layer) or on one side of a four-layer, 4 × 4 Ag(100) periodic slab (16 atoms/layer), with ~12 Å vacuum in the surface normal direction to isolate the slabs from their periodic images. (The $n \times n$ nomenclature refers to the number of repeated primitive lattice vectors that comprise the supercell in each direction within the surface plane.) The periodic slabs were constructed using the PAW–DFT–LDA equilibrium lattice parameter of face-centered cubic bulk Ag (4.015 Å), which is in reasonable agreement with the experimental value of 4.085 Å [35].

The total energies were converged to 1 meV/atom with a plane wave basis kinetic energy cutoff of 800 eV and Monkhorst–Pack [36] k-point sampling of 5 × 5 × 1 for each supercell. We employed the Methfessel–Paxton [37] second-order smearing method for Brillouin zone integration, with a Fermi surface smearing width of 0.2 eV. The error associated with this level of smearing is estimated to be <0.1 meV/atom.

Relaxing the Co atom and the top two Ag surface layers until the forces on the atoms were less than 0.05 eV Å^{-1} changed the total energy by <1.2 meV/atom compared to the structure where only the Co atom position was optimized. We therefore kept the Ag surface atoms at bulk-terminated positions and used the optimized Co–surface distances of 1.86 Å on Ag(111) and 1.49 Å on Ag(100).

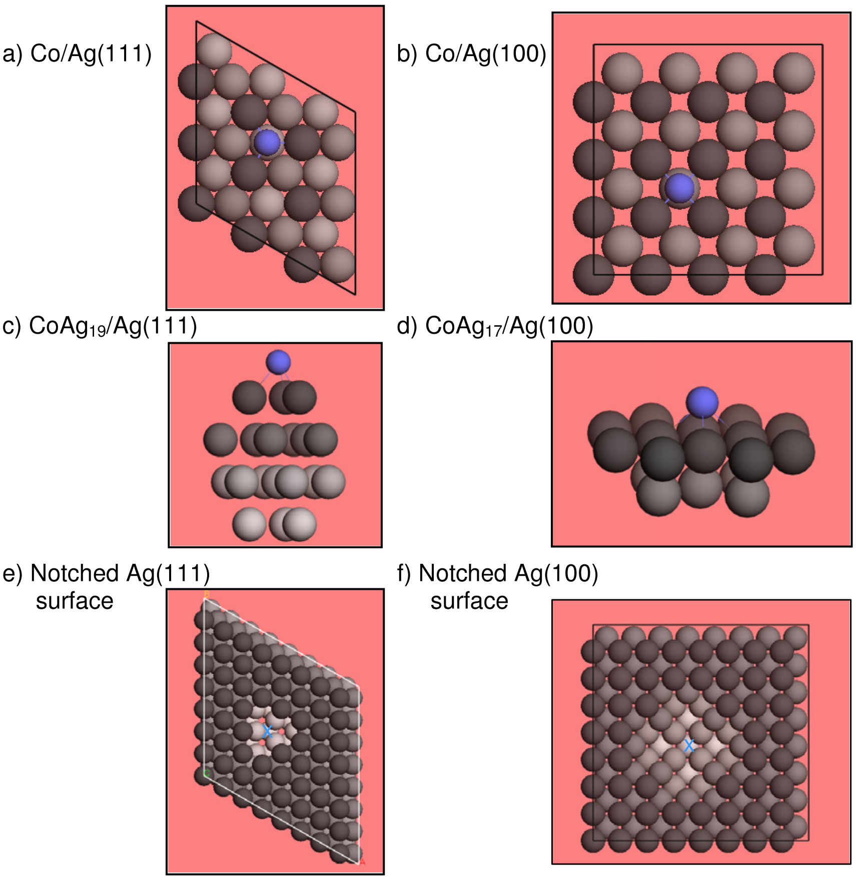

Figure 1. Co (in blue) adsorbed on (a) 3 × 3 Ag(111) periodic slab and (b) 4 × 4 Ag(100) periodic slab for SP-DFT calculations used to optimize the geometric structure and to obtain the DFT ground state spin structure for comparison. Co adsorbed on (c) an Ag_{19} cluster representing the (111) surface and (d) an Ag_{17} cluster representing the (100) surface in the embedded CASSCF calculations. The clusters are embedded into 8 × 8 notched slabs, where the cluster is carved out of each surface, as illustrated in (e) for a six-layer Ag(111) periodic slab and (f) a four-layer Ag(100) periodic slab. The × (in blue) marks the center of the removed cluster. The Ag atoms are scaled in color, with the color gradually going to lighter shades of gray with increasing surface depth.

(This figure is in colour only in the electronic version)

3.2. ECW calculations

The CASSCF [38] method captures the static correlation effects required to properly describe a many-electron open-shell singlet and the near-degeneracies of various Co d-electron configurations. Here, the many-electron wavefunction is expanded in a basis of spin-adapted Slater determinants that correspond to all possible electronic excitations within a chosen set of valence electrons and orbitals (defining the active space). The molecular orbitals (MOs) that constitute the Slater determinants are formed from a linear combination of Gaussian atomic orbitals (AOs). Both CI expansion coefficients for the Slater determinants and AO coefficients for the MOs are optimized variationally. Convergence of the CASSCF active space is established by a series of CASSCF calculations in which the size of the active space is systematically increased until no additional configurations with weight $|c_i|^2 > 0.01$ appear in the CASSCF wavefunction.

ECW calculations, in particular embedded CASSCF calculations, were performed on $CoAg_{19}$ and $CoAg_{17}$ (figures 1(c) and (d)) embedded into six-layer Ag(111) and four-layer Ag(100) 8 × 8 slabs (i.e. 64 atoms/layer), respectively. $CoAg_{19}$ has three Ag atoms in the surface layer, six in the second layer, seven in the third and three in the fourth. $CoAg_{17}$ has twelve Ag atoms in the surface layer and five in the second layer. We study clusters with an even number of electrons in order to allow for the possible formation of the non-magnetic singlet Kondo ground state. Earlier work had shown these morphologies and sizes of clusters to be sufficient to converge the electronic structure of the impurity and its neighboring atoms [22]. The particular cluster structures are chosen to retain the symmetries of the surfaces, which is C_{3v} for Ag(111) and C_{4v} for Ag(100). The atomic structure of each cluster is kept to the DFT-optimized geometry of the periodic slab. Due to the large size of these clusters, we use larger supercells than employed in the DFT calculations used to determine structures, so as to isolate the clusters from their images in the ECW calculations. The background densities, ρ_{II}, are obtained from PAW–DFT–LDA calculations on notched slabs (figures 1(e) and (f)) in which the corresponding atoms in the clusters are removed from the adsorbate/surface six- and four-layer 8 × 8 slab models defined above.

The core electrons and nuclei of the Co adatom and Ag atoms nearest to Co are represented by Hay–Wadt effective core potentials (ECPs) and the valence orbitals are expanded in Gaussian basis sets to describe the 4s and 3d electrons of Co and the 5s and 4d electrons of Ag [39]. Due to the large size of these clusters, one-electron ECPs treating only the Ag 5s as valence and corresponding basis sets are employed for non-nearest-neighbor Ag atoms [40].

Embedded CASSCF calculations were performed using our modified version of the MOLCAS [41] quantum chemistry package, MOLCAS-EMBED. For $\mathrm{CoAg_{19}}$, the converged CASSCF active space has 12 electrons distributed over 14 orbitals, which roughly involves two Co d-electrons in two orbitals and 10 Co/Ag sp-electrons in 12 orbitals. The other Co d-electrons never enter the active space and remain in doubly occupied orbitals. Additional orbitals beyond the number of electrons are required in this case in order to include degenerate pairs to preserve the overall point group symmetry. For $\mathrm{CoAg_{17}}$, the converged CASSCF active space is 14 electrons in 14 orbitals, which correspond to eight Co d-electrons in eight orbitals and six sp-electrons in six orbitals. For this cluster, it was necessary to correlate all d-electrons in order to verify the d-electronic structure, in contrast to $\mathrm{CoAg_{19}}$ in which the majority of d-electrons on Co did not require a correlated description.

Cluster size convergence of the results (in our case, the Co d-electronic structure) is established by expanding the cluster to include more and more metal atoms until the results no longer change. Cluster size convergence tests for Co on Cu surfaces found an embedded $\mathrm{CoCu_7}$ representation for Co on the (111) surface and $\mathrm{CoCu_{13}}$ representation for Co on the (100) surface to be sufficient [21, 22]. We verified that Co/Ag displays similar convergence behavior by examining smaller clusters such as $\mathrm{CoAg_7}$ embedded in Ag(111); however, we report results for larger clusters for which not only the d-electronic structure but the spin state excitation energies are converged as well. In particular, the Kondo singlet ground state is associated with a set of low energy spin excitations of the order of $k_\mathrm{B}T_\mathrm{K}$ (~3.5 meV on Ag(100) [11] and ~8 meV on Ag(111) [10]). Although cluster size convergence of the d-electronic structure is achieved at small cluster sizes, we ultimately studied the larger clusters for which the sp-band is dense enough that we are also able to capture the small energies associated with spin flips of metal electrons.

4. Results and analysis

For purposes of comparison, we first calculated the magnetic ground state of Co adatoms on Ag(111) and Ag(100) surfaces with SP-DFT using the periodic slab models shown in figures 1(a) and (b). To determine the lowest energy spin state, initial guesses for the Co magnetic moments of 0.0, 2.0 and 4.0 μ_B were used on each surface. The Co–surface distance was optimized for each initial magnetic moment; this distance was found to be relatively insensitive to spin state, varying by at most 0.14 Å on both surfaces. The equilibrium ground states have net magnetic moments of 2.22 μ_B for Co/Ag(111) and 1.67 μ_B for Co/Ag(100), roughly corresponding to triplet ground states, with net spin polarization localized on the Co adatom, consistent with previous SP-DFT calculations for Co on other coinage metal surfaces [20, 42, 43]. Thus, as expected based on our earlier discussion, SP-DFT does not reproduce the magnetic quenching at low temperatures characteristic of the Kondo state.

The crystal field of the Ag surface breaks the degeneracy of the Co adatom's d-orbitals in a manner specific to the symmetry of the surface. On the (111) surface, the five d-orbitals are split into two doubly degenerate pairs with e-symmetry, (d_{xy}, d_{x2-y2}) and (d_{xz}, d_{yz}), and one with $\mathrm{a_1}$ symmetry (d_{z2}). On the (100) surface, the orbitals are split into one e-pair (d_{xz}, d_{yz}), one $\mathrm{a_1}$ (d_{z2}), one $\mathrm{b_1}$ (d_{xy}) and one $\mathrm{b_2}$ (d_{x2-y2}). The splitting of the d-orbitals, the Co coordination number and the Co–metal bond length all influence the d-electronic structure of the impurity, which in turn influences the nature of the Kondo resonance wavefunction, as discussed further below.

We analyze the embedded CASSCF wavefunctions and Co d-structures of $\mathrm{CoAg_{19}}$ and $\mathrm{CoAg_{17}}$, respectively embedded into the Ag(111) and Ag(100) periodic surface slabs as described earlier. The dominant configurations and weights ($|c_i|^2$) of the singlet, triplet and quintet wavefunctions are presented in table 2. Symmetry equivalent configurations are not shown, though their contribution to the weight is taken into account. As noted previously [21], the large deviation from unity of the dominant configuration's weight is consistent with the strongly correlated nature of the Kondo state. The wavefunction is open shell on both surfaces, with two open-shell d-electrons on Co that are spin-compensated by the surrounding Ag metal electrons to form an overall singlet state, similar to the anti-ferromagnetic coupling assumed by Kondo long ago. The existence of two unpaired electrons on Co corresponds to an $S = 1$ impurity; in general, it has been shown that full screening of an $S = 1$ Kondo state impurity requires coupling to two independent metallic bands [1]. Our ECW wavefunction is consistent with this picture in that the unpaired d-electrons on Co couple to metallic Ag sp-delocalized orbitals/bands from different symmetries (e_x and e_y), providing further evidence that we are interrogating a Kondo state. We also find that spin-flip excitation energies are small on both surfaces: energy differences between singlet, triplet and quintet states are <0.1 eV, which is within the error inherent in our calculations (~0.1 eV) and is consistent with the expected near-degeneracies for spin-flip excitations in Kondo systems.

Note that the *ab initio* ECW theory is distinguished from model Hamiltonian approaches in that the ECW is an explicit many-body wavefunction, and not readily mapped onto the usual single-particle picture. While natural orbitals can be derived from a many-body wavefunction, unique orbital energies are not available. Thus, single-particle quantities such as the density of states, the Fermi energy and sum rules cannot be obtained from the ECW and corroborated with some known aspects of Kondo behavior. However, the objective here is in understanding the nature of the Kondo state near the impurity, and other evidence suggests that a local description is sufficient for this purpose. As discussed in section 1, the Kondo temperature (and therefore the Co–metal hybridization) has been shown to depend strongly on the local environment [30, 31]. The ECW captures the strong, short-range correlation effects that lead to hybridization and singlet

Table 2. Dominant configurations with weight $|c_i|^2 \geqslant 0.1$ of the embedded CASSCF wavefunctions for different spin states of $CoAg_{19}$ and $CoAg_{17}$.

	Spatial configuration	Weight[a]
$CoAg_{19}$/Ag(111)		
Singlet[b]	$(1a_1)^2(1e_x)^2(1e_y)^1(2e_x)^1(2e_y)^1(3e_x)^1$	0.42
	$(1a_1)^1(1e_x)^2(1e_y)^2(2e_x)^1(2e_y)^1(3e_x)^1$	0.23
Triplet[b]	$(1a_1)^2(1e_x)^2(1e_y)^1(2e_x)^1(2e_y)^1(3e_x)^1$	0.63
Quintet[b]	$(1a_1)^2(1e_x)^2(1e_y)^1(2e_x)^1(2e_y)^1(3e_x)^1$	0.42
	$(1a_1)^1(1e_x)^2(1e_y)^2(2e_x)^1(2e_y)^1(3e_x)^1$	0.23
$CoAg_{17}$/Ag(100)		
Singlet[c]	$(1a_1)^2(1b_1)^1(1e_x)^2(1e_y)^2(2e_x)^1(2e_y)^2$	0.26
	$(1a_1)^2(1b_1)^1(1e_x)^2(1e_y)^1(2e_x)^2(2e_y)^1(3e_x)^1$	0.20
Triplet[c]	$(1a_1)^2(1b_1)^1(1e_x)^2(1e_y)^2(2e_x)^1(2e_y)^2$	0.28
	$(1a_1)^2(1b_1)^1(1e_x)^2(1e_y)^1(2e_x)^2(2e_y)^1(3e_x)^1$	0.20
Quintet[c]	$(1a_1)^1(1b_1)^1(1e_x)^1(1e_y)^1(2e_x)^2(2e_y)^2(3e_x)^1(3e_y)^1$	0.75
	$(1a_1)^1(1b_1)^1(1e_x)^1(1e_y)^2(2e_x)^2(2e_y)^2(3e_x)^1$	0.20

[a] Weight $|c_i|^2$ corresponds to the sum over all symmetry equivalent configurations, only one of which is shown.

[b] The 1e, 3e and $1a_1$ orbitals are linear combinations of Co/Cu sp-orbitals while the 2e orbitals are a mixture of doubly degenerate Co d- and Co/Cu sp-orbitals.

[c] The 1e, 2e, 3e and $1a_1$ are mixtures of Co d- and Co/Cu sp-orbitals, while the $1b_1$ orbital has only Co d-character.

coupling between the Co and metal, and is consistent with the two-band behavior expected for the screening of an $S = 1$ impurity, as mentioned above. The rapid convergence of the Co d-electronic structure with respect to cluster size (section 3) indicates that this quantity is very sensitive to and determined by the local environment only. While quantitative errors in the energies may arise due to numerics (e.g. finite basis set, approximation for the frozen background, etc), the qualitative nature of the wavefunction is much more robust with respect to cluster size and numerics and hence is our focus here.

A key quantity that we are interested in and that is not well described in model Hamiltonian approaches is the Co d-electronic structure, which is derived here from a Mulliken population analysis of the many-body wavefunction's natural orbitals. The Co d-electronic structures for the singlet states of Co on Ag(111) and Ag(100) are compared with previously reported [22] ECW populations for Co on Cu(111) and Cu(100) in table 3. The Co d-occupations are essentially the same for all three spin states of Co on Cu(111), Cu(100) and Ag(111). For Co on Ag(100), the quintet d-occupation is different than the singlet or the triplet, with the d_{z2} orbital singly occupied and the d_{xz} and d_{yz} both doubly occupied. Since we are concerned primarily with understanding the actual Kondo ground state, we focus our analysis on the singlet.

Table 3. d-electronic structure of Co adatoms on Cu and Ag surfaces.

	d_{x2-y2}	d_{xy}	d_{xz}	d_{yz}	d_{z2}
$CoAg_{19}$/Ag(111)	1.6	1.6	1.4	1.4	2.0
$CoAg_{17}$/Ag(100)[a]	1.0	2.0	1.3	1.7	1.9
	1.0	2.0	1.7	1.3	1.9
$CoCu_{19}$/Cu(111)[b]	1.6	1.6	1.4	1.4	2.0
$CoCu_{17}$/Cu(100)[b]	2.0	1.0	2.0	2.0	1.0

[a] This state is doubly degenerate; the d-structures for both states are shown.

[b] Reference [22].

The aspect of the calculated d-structure most relevant to Kondo behavior is the character of the d-orbitals that gives rise to the local impurity moment; for the STM experiments, a local moment due to single occupation of a Co d_{z2} orbital is expected to couple most strongly to the STM tip states (discussed further below). This d_{z2} orbital is predicted to be doubly occupied for Co on Ag(111), Ag(100) and Cu(111) but singly occupied on Cu(100). At first this trend may seem counterintuitive, since Ag(100) has the same symmetry and coordination number as Cu(100) and the Co–metal bond lengths are similar for Co on Cu(100) and Ag(100). So why would the (100) surfaces of Ag and Cu induce different d-electronic structures on Co? Perhaps the trend is driven by the strength of the interaction of Co–Cu versus Co–Ag. Specifically, the interaction between same-row elements (Co and Cu) is typically stronger than those between elements with significantly differently sized orbitals (Co and Ag). If this expected trend in interaction strength is upheld here, it may explain why a change in Cu surface orientation strongly affects the Co d-structure, while a change in Ag surface orientation leaves the Co d-structure unperturbed.

To investigate whether Co–Ag interactions are weaker than Co–Cu interactions, we analyzed the occupation numbers of the bonding and anti-bonding Co–metal natural orbitals from the embedded CASSCF wavefunctions. We find lower occupation numbers of the bonding orbitals (e.g. 1.85 versus 1.95) and a stronger occupation of anti-bonding orbitals (e.g. 0.13 versus 0.05) for Co/Ag(111) versus Co/Cu(111), consistent with weaker Co–Ag interactions. (In the limit of no interaction, bonding and anti-bonding orbitals have equal occupation.) This result confirms our hypothesis above and explains the surface structure sensitivity of the d-structure for Co on Cu surfaces and the corresponding lack of surface structure sensitivity for Co on Ag surfaces.

The Co d-orbitals giving rise to the local moment can clearly be associated with the impurity level in the Anderson impurity model, and connecting back to this picture provides insight into the observed STS data [21, 22]. As discussed in section 1, the STS lineshape is characterized by the parameter q, which is typically obtained by fitting the experimental data to the lineshape expression of equation (1). Within the Anderson impurity model, a microscopic expression for q can be derived as $q = A/B$, where [6]

$$A = M_{\mathrm{at}} + \sum_{\mathbf{k}} M_{\mathbf{k}t} V_{a\mathbf{k}} P \left(\frac{1}{\varepsilon - \varepsilon_{\mathbf{k}}} \right),$$

$$B = \pi \sum_{\mathbf{k}} M_{\mathbf{k}t} V_{a\mathbf{k}} \delta(\varepsilon - \varepsilon_{\mathbf{k}}),$$

and P denotes the principal value. The various contributions to q are the conduction band energies $\varepsilon_{\mathbf{k}}$, hybridization matrix elements V and hopping matrix elements M. These matrix elements are evaluated with respect to tip states t, impurity states a and substrate conduction states $\mathbf{k}$. The STS lineshape is symmetric around the Fermi level when tip–impurity coupling is weak ($q \sim 0$) and asymmetric when both tip–substrate and tip–impurity coupling have comparable strengths ($q \sim 1$) [6]. Experiments reveal that Co on Cu(111), Ag(111) and Ag(100) display the former lineshape while Co on Cu(100) displays the latter lineshape.

Our *ab initio* ECWs for Co on metal substrates tell us specifically the symmetry of the impurity d-orbitals that are involved in Kondo behavior, and how this changes with respect to variations in the local environment. It is the symmetry of these orbitals that determines whether the tip–impurity matrix elements are large or small, thus controlling the extent of the contribution from tip–impurity terms to q. Tip states are expected to be dominated by s-waves [44] and therefore should couple most strongly to orbitals with a_1 symmetry, i.e. Co d_{z2} or d_{z2} + sp hybrid orbitals. For Co on Cu(100), the ECW calculations reveal that the impurity moment resides in two d-orbitals, one of which is d_{z2} that has the correct symmetry to couple strongly with tip states. Thus, both tip–impurity and tip–substrate matrix elements contribute to give $q \sim 1$, as seen in experiments. Conversely, our *ab initio* approach allows for the possibility that the relevant impurity orbitals could have the wrong symmetry for strong coupling with tip states. This is seen here for Co on Cu(111), Ag(111) and Ag(100), where the impurity moment resides in two d-orbitals other than the d_{z2} and thus explains why experiments find $q \sim 0$ in these cases. This is a point that has been missed in previous model Hamiltonian analyses of the STM experiments, where the impurity level is always assumed to be a d_{z2} orbital.

5. Conclusions

In summary, ECW calculations of Co adatoms on Cu and Ag surfaces offer an explanation for the observed trends in STS lineshapes, which in turn are directly related to tunneling pathways that probe the nature of the Kondo state. Earlier work by Huang and Carter already revealed that the differing lineshapes observed for Co on Cu(100) and Cu(111) were due to changes in the impurity d-electronic structure that comprises the Kondo singlet on these two surfaces. The current work provides insights into the puzzling trend that the Kondo state is sensitive to surface orientation only on Cu surfaces but not on Ag surfaces, with the origin being the stronger interaction between Co and Cu compared to Co and Ag. The stronger interaction between Co and Cu, coupled with the change in coordination number on different surface facets, induces a change in the Co d_{z2} orbital occupation that is responsible for the drastic change in lineshape observed for Co/Cu(111) compared to Co/Cu(100). In contrast, the weaker interaction between Co and Ag leaves the Co d_{z2} orbital occupation unchanged upon changing surface symmetry, as manifested in the similar tunneling lineshapes observed for Co/Ag(111) and Co/Ag(100).

Acknowledgments

We would like to thank Professors Peter Nordlander and Alexander Schneider for useful discussions and are grateful for the financial support of the Department of Energy, Basic Energy Sciences.

References

[1] Hewson A C 1993 *The Kondo Problem to Heavy Fermions* (*Cambridge Studies in Magnetism*) (Cambridge: Cambridge University Press)
[2] Kondo J 1964 *Prog. Theor. Phys.* **32** 37
[3] Heeger A J 1969 *Solid State Physics* vol 23, ed F Seitz, D Turnbull and H Ehrenreich (New York: Academic) p 283
[4] Li J, Schneider W-D, Berndt R and Delley B 1998 *Phys. Rev. Lett.* **80** 2893
[5] Madhavan V, Chen W, Jamneala T, Crommie M F and Wingreen N S 1998 *Science* **280** 567
[6] Madhavan V, Chen W, Jamneala T, Crommie M F and Wingreen N S 2001 *Phys. Rev.* B **64** 165412
[7] Berndt R, Li J, Schneider W-D and Delley B 1999 *Phys. Status Solidi* **215** 845
[8] Fano U 1961 *Phys. Rev.* **124** 1866
[9] Knorr N, Schneider M A, Diekhöner L, Wahl P and Kern K 2002 *Phys. Rev. Lett.* **88** 096804
[10] Schneider M A, Vitali L, Knorr N and Kern K 2002 *Phys. Rev.* B **65** 121406
[11] Wahl P, Diekhöner L, Schneider M A, Vitali L, Wittich G and Kern K 2004 *Phys. Rev. Lett.* **93** 176603
[12] Anderson P W 1961 *Phys. Rev.* **124** 41
[13] Plihal M and Gazduk J W 2001 *Phys. Rev.* B **63** 085404
[14] Merino J and Gunnarsson O 2004 *Phys. Rev. Lett.* **93** 156601
[15] Lin C-Y, Castro Neto A H and Jones B A 2006 *Phys. Rev. Lett.* **97** 156102
[16] Ujsaghy O, Kroha J, Szunyogh L and Zawadowski A 2000 *Phys. Rev. Lett.* **85** 2557
[17] Schiller A and Hershfield S 2000 *Phys. Rev.* B **61** 9036
[18] Barral M A, Llois A M and Aligia A A 2004 *Phys. Rev.* B **70** 035416
[19] Roura-Bas P, Barral M A and Llois A M 2009 *Phys. Rev.* B **79** 075410
[20] Huang P and Carter E A 2006 *J. Chem. Phys.* **125** 084102
[21] Huang P and Carter E A 2006 *Nano Lett.* **6** 1146
[22] Huang P and Carter E A 2008 *Nano Lett.* **8** 1265
[23] Govind N, Wang Y A, da Silva A J R and Carter E A 1998 *Chem. Phys. Lett.* **295** 129
[24] Govind N, Wang Y A and Carter E A 1999 *J. Chem. Phys.* **110** 7677
[25] Klüner T, Govind N, Wang Y A and Carter E A 2001 *Phys. Rev. Lett.* **86** 5954
[26] Klüner T, Govind N, Wang Y A and Carter E A 2002 *Phys. Rev. Lett.* **88** 209702

[27] Klüner T, Govind N, Wang Y A and Carter E A 2002 *J. Chem. Phys.* **116** 42
[28] Sharifzadeh S, Huang P and Carter E A 2008 *J. Phys. Chem.* C **112** 4649
[29] Sharifzadeh S, Huang P and Carter E A 2009 *Chem. Phys. Lett.* **470** 347
[30] Schneider M A, Vitali L, Wahl P, Knorr N, Diekhöner L, Wittich G, Vogelgesang M and Kern K 2005 *Appl. Phys.* A **80** 937
[31] Schneider M A, Wahl P, Diekhöner L, Vitali L, Wittich G and Kern K 2005 *Japan. J. Appl. Phys.* **44** 5328
[32] Blöchl P E 1994 *Phys. Rev.* B **50** 17953
[33] Perdew J P and Zunger A 1981 *Phys. Rev.* B **23** 5048
[34] Kresse G and Joubert D 1999 *Phys. Rev.* B **59** 1758
[35] Liu L-G and Bassett W A 1973 *J. Appl. Phys.* **44** 1475
[36] Monkhorst H J and Pack J D 1976 *Phys. Rev.* B **13** 5188
[37] Methfessel M and Paxton A T 1989 *Phys. Rev.* B **40** 3616
[38] Roos B O, Taylor P R and Siegbahn P E M 1980 *Chem. Phys.* **48** 157
[39] Hay P J and Wadt W R 1985 *J. Chem. Phys.* **82** 270
[40] Hay P J and Martin R L 1985 *J. Chem. Phys.* **83** 5174
[41] Karlström G *et al* 2003 *Comput. Mater. Sci.* **28** 222
[42] Lang P, Stepanyuk V S, Wildberger K, Zeller R and Dederichs P H 1994 *Solid State Commun.* **92** 755
[43] Weissmann M and Llois A M 2001 *Phys. Rev.* B **63** 113402
[44] Lang N D 1986 *Phys. Rev.* B **34** 5947